APPLIED AND ENVIRONMENTAL MICROBIOLOGY, Mar. 2007, p. 1712–1720 Vol. 73, No. 6
0099-2240/07/$08.00+0 doi:10.1128/AEM.02218-06

Does the Antibacterial Activity of Silver Nanoparticles Depend on the Shape of the Nanoparticle? A Study of the Gram-Negative Bacterium *Escherichia coli*[▽]

Sukdeb Pal, Yu Kyung Tak, and Joon Myong Song*

Research Institute of Pharmaceutical Sciences and College of Pharmacy, Seoul National University, Seoul 151-742, South Korea

Received 21 September 2006/Accepted 9 January 2007

In this work we investigated the antibacterial properties of differently shaped silver nanoparticles against the gram-negative bacterium *Escherichia coli*, both in liquid systems and on agar plates. Energy-filtering transmission electron microscopy images revealed considerable changes in the cell membranes upon treatment, resulting in cell death. Truncated triangular silver nanoplates with a {111} lattice plane as the basal plane displayed the strongest biocidal action, compared with spherical and rod-shaped nanoparticles and with Ag^+ (in the form of $AgNO_3$). It is proposed that nanoscale size and the presence of a {111} plane combine to promote this biocidal property. To our knowledge, this is the first comparative study on the bactericidal properties of silver nanoparticles of different shapes, and our results demonstrate that silver nanoparticles undergo a shape-dependent interaction with the gram-negative organism *E. coli*.

Over the past few decades, inorganic nanoparticles, whose structures exhibit significantly novel and improved physical, chemical, and biological properties, phenomena, and functionality due to their nanoscale size, have elicited much interest. Nanophasic and nanostructured materials are attracting a great deal of attention because of their potential for achieving specific processes and selectivity, especially in biological and pharmaceutical applications (5, 39).

Discoveries in the past decade have demonstrated that the electromagnetic, optical, and catalytic properties of noble-metal nanocrystals are strongly influenced by shape and size (6, 26). This has motivated an upsurge in research on the synthesis routes that allow better control of shape and size (18, 34, 41), with projected applications in nanoelectronics and spectroscopy (14, 19, 36).

Recent studies have demonstrated that specially formulated metal oxide nanoparticles have good antibacterial activity (33), and antimicrobial formulations comprising nanoparticles could be effective bactericidal materials (11, 12).

Among inorganic antibacterial agents, silver has been employed most extensively since ancient times to fight infections and control spoilage. The antibacterial and antiviral actions of silver, silver ion, and silver compounds have been thoroughly investigated (28, 29, 37). However, in minute concentrations, silver is nontoxic to human cells. The epidemiological history of silver has established its nontoxicity in normal use. Catalytic oxidation by metallic silver and reaction with dissolved monovalent silver ion probably contribute to its bactericidal effect (17). Microbes are unlikely to develop resistance against silver, as they do against conventional and narrow-target antibiotics, because the metal attacks a broad range of targets in the organisms, which means that they would have to develop a host of mutations simultaneously to protect themselves. Thus, silver ions have been used as an antibacterial component in dental resin composites (15), in synthetic zeolites (22), and in coatings of medical devices (2).

Recent literature reports encouraging results about the bactericidal activity of silver nanoparticles of either a simple or composite nature (21, 31). Elechiguerra and coworkers (9) found that silver nanoparticles undergo a size-dependent interaction with human immunodeficiency virus type 1, preferably via binding to gp120 glycoprotein knobs. The size-dependent interaction of silver nanoparticles with gram-negative bacteria has also been reported by the same group (25). However, little is known about how the biological activity of silver nanoparticles changes as the shape of the particles changes.

For these reason, we investigated the shape dependence of the antibacterial activity of silver nanoparticles against *Escherichia coli*. Silver nanoparticles of different shapes were synthesized by solution phase routes, and their interactions with *E. coli* were studied. Energy-filtering transmission electron microscopy (EFTEM) was used as a complementary technique to examine the treated cells. The size-dependent antimicrobial activity of silver nanoparticles has already been investigated (9, 25), while to our knowledge the effect of shape on the antibacterial activity of silver nanoparticles has not been reported previously.

MATERIALS AND METHODS

Materials. *E. coli* (ATCC 10536) was obtained from the American Type Culture Collection (Manassas, VA). Difco nutrient broth (NB) (BD234000) and Difco nutrient agar (BD 213000) medium (Becton Dickinson and Co.) were used to grow and maintain the bacterial cultures per the supplier's protocol. Chemicals such as silver nitrate, ascorbic acid, sodium citrate tribasic dihydrate, and cetyltrimethyl ammonium bromide (CTAB) were of the highest purity available (Sigma). These reagents were used as received without further purification.

Preparation of silver nanoparticles. The silver nanoparticles used in this work were synthesized by two different methods. Both include seeding and growth.

First, silver seeds were prepared by rapidly injecting 0.5 ml of 10 mM $NaBH_4$ into an aqueous solution (with continuous stirring) containing 0.5 ml of 0.01 M

* Corresponding author. Mailing address: Research Institute of Pharmaceutical Sciences and College of Pharmacy, Seoul National University, Seoul 151-742, South Korea. Phone: 82-2-880-7841. Fax: 82-2-871-2238. E-mail: jmsong@snu.ac.kr.

▽ Published ahead of print on 19 January 2007.

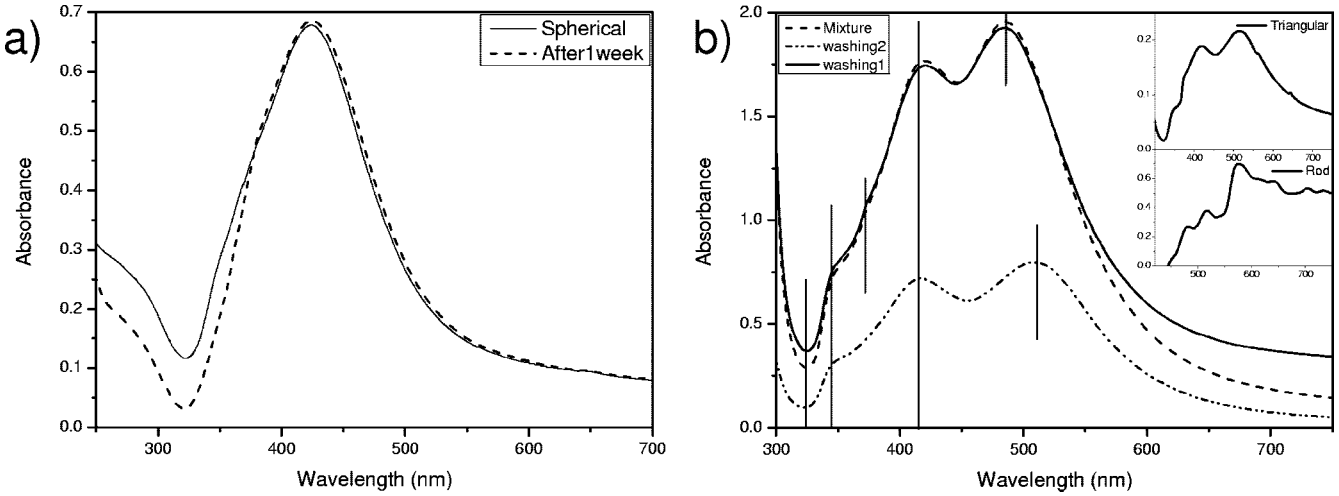

FIG. 1. (a) Absorption spectra of solutions containing spherical silver nanoparticle recorded immediately after precipitation and after 1 week. (b) Absorption spectra of reaction mixtures containing elongated (rod-shaped) and truncated triangular silver nanoplates and other anisotropic silver nanoparticles and the first and second wash liquor (centrifuge). (Top inset) Absorption spectrum of solution containing purified truncated triangular silver nanoplates. (Bottom inset) UV-visible spectrum of the solution containing rod-shaped particles with larger aspect ratios.

$AgNO_3$ and 20 ml of 0.001 M sodium citrate. The resultant solution was stirred for ~5 min and aged for 1.5 h.

In the first method, the spherical silver hydrosols were prepared by reducing aqueous $AgNO_3$ with sodium citrate at near-boiling temperature. In a typical procedure, an aqueous solution of $AgNO_3$ (100 ml, 0.001 M) was brought to boiling, and then 3 ml of the silver seed solution and an aqueous solution of sodium citrate were added so that the final concentration of sodium citrate in the reaction mixture became 0.001 M. The solution was heated until the color was greenish yellow. The solution was cooled to room temperature. The silver nanoparticles were purified by centrifugation. To remove excess silver ions, the silver pellet was washed three times with deionized water. A dried powder of the nanosize silver was obtained by freeze-drying. To carry out interaction of the silver nanoparticles with bacteria, the silver nanoparticle powder in the freeze-drying cuvette was resuspended in water; the suspension was homogenized with a Branson 2200 ultrasonicator. The resulting silver concentration was measured by either inductively coupled plasma (ICP) emission spectroscopy (ES) (ICPS-1000IV; Shimadzu, Kyoto, Japan) or ICP mass spectrometry (MS) (ELAN 6100; Perkin-Elmer SCIEX).

Elongated (rod-shaped) and truncated triangular silver nanoplates were synthesized by a solution phase method for the large-scale preparation of truncated triangular nanoplates (8). To the particle growth solution containing 5 ml of 0.01 M $AgNO_3$, 10 ml of 0.1 M ascorbic acid, 146 ml of 0.1 M CTAB, and 5 ml of silver seeds, 1 ml of 1 M NaOH was added to accelerate particle growth. The solution color changed from light yellow to brown, red, and green within a few minutes. The resultant solution was aged at 21°C for 12 h, 35°C for 5 min, and 21°C for 24 h. The color of the aged solution changed from green to red.

The silver nanoplates were purified by centrifugation. The surfactants and the smaller particles were separated by centrifugation at 2,100 × *g* for 10 min. The resultant precipitate was suspended in water and centrifuged again at 755 × *g* for 10 min. Finally, the precipitate was suspended in water, and rods with larger aspect ratios were removed by centrifuging at 84 × *g* for 10 min. The supernatant solution contained the truncated triangular silver nanoplates. It was not possible to quantify the precipitate by weight, as it was always associated with some water. The resulting silver level was quantified by ICP-ES or ICP-MS analysis and reported in milligrams per liter or parts per million (detection limit of Ag, >0.1 ppb).

Organism preparation. *E. coli* ATCC 10536 was grown overnight in NB at 37°C. Washed cells were resuspended in NB, and optical density (OD) was adjusted to 0.1, corresponding to 10^8 CFU/ml at 600 nm.

Bacterial growth or killing kinetics in presence of nanosilver. To examine the bacterial growth or killing kinetics in the presence of silver nanoparticles, *E. coli* cells were grown in 100 ml of NB supplemented with different doses of nanosilver (total silver content, 1, 6, 12, 12.5, 50, or 100 μg), at 37°C with continuous agitation. The cylindrical sample containers were placed horizontally on an orbital shaker platform and agitated at 225 rpm. Growth or killing rates and bacterial concentrations were determined by measuring OD at 600 nm. The OD values were converted into concentration of *E. coli* cells (CFU per milliliter) (21, 31). OriginPro 7.5 software was used to analyze the experimental data and for graphing (see Fig. 1 and 3 to 7).

Bacterial susceptibility to nanosilver. To examine the susceptibility of *E. coli* to different silver nanoparticles, nutrient agar plates from a solution of agar were prepared. A 100-μl sample of bacterial suspension cultured in NB (with a concentration of 10^5 or 10^7 CFU/ml of *E. coli*) was plated on a nutrient agar plate. The plates were then supplemented with different amounts of nanosize silver particles (1 to 100 μg), and the plates were incubated further at 37°C. The numbers of resultant colonies were counted after 24 h of incubation. Silver-free plates incubated under the same conditions were used as controls. The counts from three independent experiments corresponding to a particular sample were averaged.

EFTEM analysis was also carried out to examine sections of the treated bacteria. Images of negatively stained particles were acquired as follows. Concentrated aqueous suspensions of *E. coli* cells were deposited on Formvar-coated grids and allowed to sit for a few minutes. The grids were exposed to aqueous 1% phosphotungstic acid for 30 s. The residual staining solution was then removed, and the samples were immediately transferred to a microscope for inspection. EFTEM images were acquired on a LIBRA 120 (Carl Zeiss) transmission electron microscope.

Characterization of silver nanoparticles. The synthesized nanoparticles were characterized by UV-visible spectroscopy and EFTEM. EFTEM images were observed with a LIBRA 120 (Carl Zeiss) transmission electron microscope. The samples were prepared by placing a drop of homogeneous suspension on a copper grid with a lacey carbon film and allowing it to dry in air. Mean particle size was analyzed from the digitized images with Image Tool software. UV-visible absorption spectra were recorded with an Optizen 2120 UV-visible spectrophotometer (Mecasys, Daejeon, Korea) with a 1-cm quartz cell.

RESULTS

UV-visible spectroscopy is one of the most widely used techniques for structural characterization of silver nanoparticles. The absorption spectrum (Fig. 1a) of the pale yellow silver colloids prepared by citrate reduction showed a surface plasmon absorption band with a maximum of ~420 nm, indicating the presence of lone spherical or roughly spherical Ag nanoparticles, and TEM imaging confirmed this (Fig. 2A). A minimum at ~320 nm corresponds to the wavelength at which the

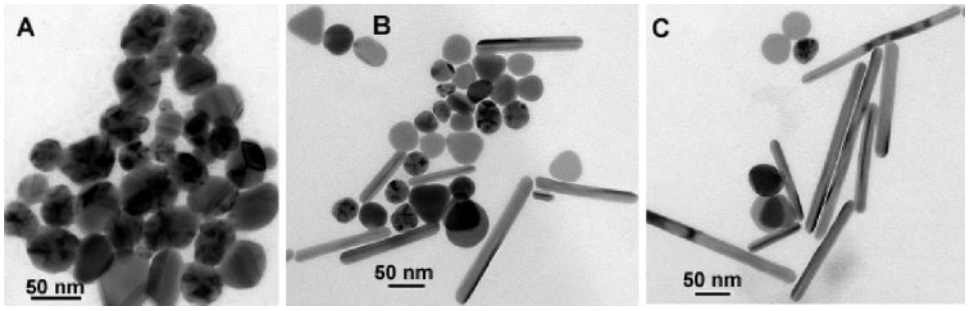

FIG. 2. EFTEM images of silver nanoparticles. (A) Spherical nanoparticles synthesized by citrate reduction. (B) Silver nanoparticles of different shapes. (C) Purified rod-shaped nanoparticles.

real and imaginary parts of the dielectric function of silver almost vanish (32).

The optical absorption spectra of metal nanoparticles are dominated by surface plasmon resonances (SPR), which shift to longer wavelengths with increasing particle size (4). The position and shape of plasmon absorption of silver nanoclusters are strongly dependent on the particle size, dielectric medium, and surface-adsorbed species (20, 26). According to Mie's theory (24), only a single SPR band is expected in the absorption spectra of spherical nanoparticles, whereas anisotropic particles could give rise to two or more SPR bands depending on the shape of the particles. The number of SPR peaks increases as the symmetry of the nanoparticle decreases (32). Thus, spherical nanoparticles, disks, and triangular nanoplates of silver show one, two, and more peaks, respectively.

Even after several days, the aqueous dispersion of freeze-dried Ag nanoparticles, prepared by citrate reduction, displayed UV-visible spectral characteristics of spherical Ag nanoparticles (Fig. 1a), confirming the colloidal stability and uniformity of the silver hydrosol.

On the other hand, interesting optical signatures were observed for the sample synthesized by the soft template method in the presence of CTAB micelles. The solution showed a red color; the corresponding absorption spectrum (Fig. 1b, "mixture" curve) displays three peaks at 348, 420, and 485 and a shoulder at 373 nm. The silver nanoparticles were separated by centrifugation. The UV-visible spectra of all centrifuged samples are also shown in Fig. 1b (curves for washing 1 and washing 2). After centrifugation, the first and second wash liquors showed absorption maxima similar to that of the parent solution. A broad hump could be identified at a longer wavelength (shifted to 509 nm for the second wash liquor), suggesting the possible presence of a population of anisotropic Ag particles.

The UV-visible spectrum of the solution containing truncated triangular silver nanoparticles (Fig. 1b, top inset) showed two symmetrical absorption peaks at ~418 and 514 nm. Also, a few humps can be seen at shorter (348 and 373 nm) as well as longer (562 and 643 nm) wavelengths. The calculation of Schatz and Van Duyne (30) for the triangular prisms with the discrete dipole approximation method suggests that the peaks at longer wavelengths are due to the in-plane dipole (514, 562, and 643 nm). The peak due to quadrupole plasmon resonance (~460 nm) was expected to be very weak (8) and could not be seen. The shoulders at 373 and 348 nm are out-of-plane dipole and quadrupole resonances, respectively. Formation of triangular nanoplates is thus evident from the appearance of these peaks. Chen and Carroll (8) also showed that the blue shift of the in-plane dipole resonance to a lower wavelength (514 nm), in contrast to the calculated resonance peak at 770 nm for a perfect triangular nanoplate, indicates the truncated nature of the triangular particles.

The UV-visible spectra of the solution containing the particles with larger aspect ratios (Fig. 1b, lower inset) showed three main absorption peaks at 480, 517, and 575 nm along with a few weak absorption peaks at the near-infrared (NIR) region. The absorption in the NIR region may be due to the in-plane dipole resonance mode associated with nanoplates with edge lengths greater than 100 nm (35) and the strong coupling between the nanoparticles arising from aggregation of silver nanoparticles (16, 27). Absorption peaks for plates of a given thickness at longer wavelengths are also suggested to be associated with the larger lateral size of the plates (7).

EFTEM images (Fig. 2) revealed more significant differences between these samples in terms of particle morphology. While samples prepared by citrate reduction consisted mostly of spherical nanoparticles (mean size of 39 nm) (Fig. 2A), anisotropic Ag particles (truncated triangular plates, rods, and

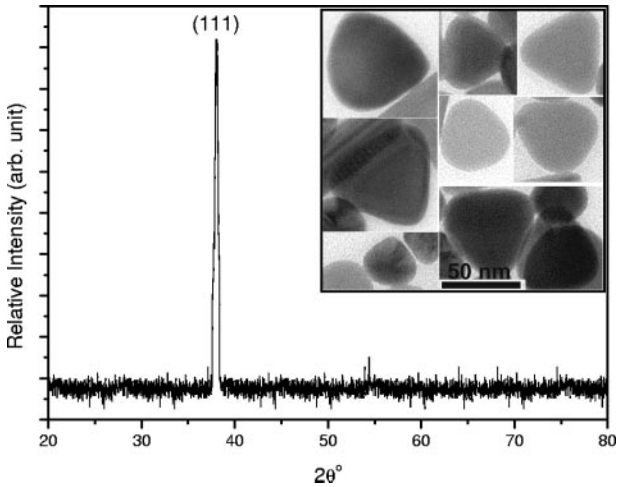

FIG. 3. OPML-XRD pattern of truncated triangular silver nanoplates. (Inset) TEM image of the purified truncated triangular particles.

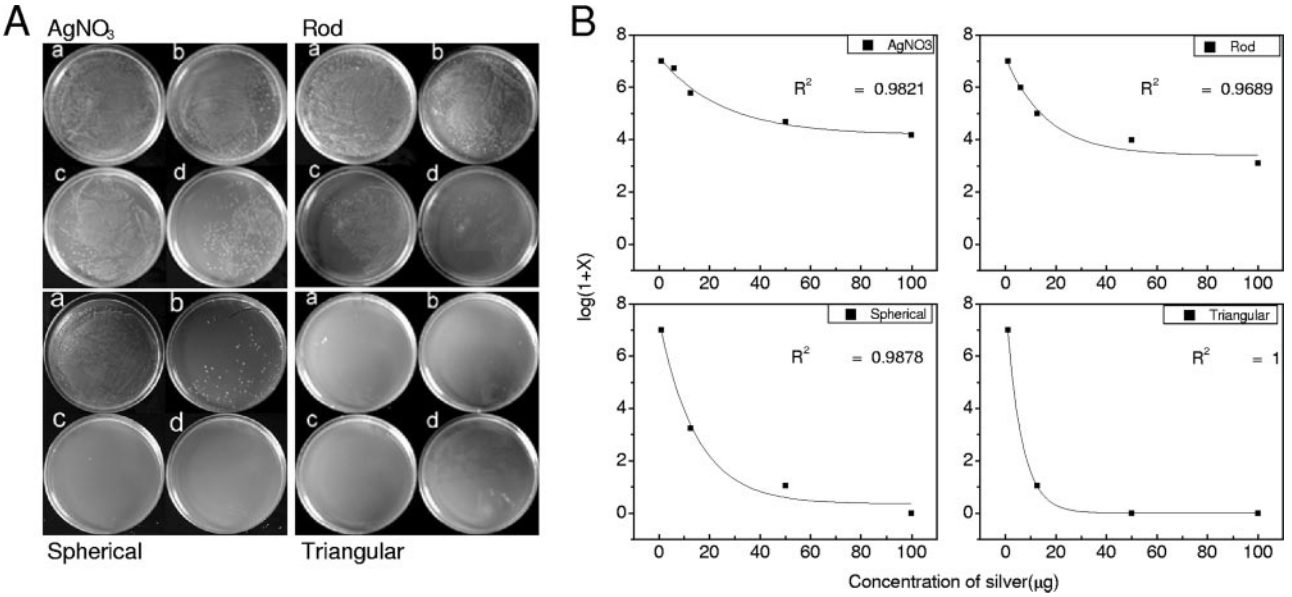

FIG. 4. (A) Petri dishes initially supplemented with 10^7 CFU/ml of *E. coli* and incubated with different forms of silver nanoparticles at (a) 1, (b) 12.5, (c) 50, and (d) 100 μg. (B) Number of *E. coli* colonies, expressed as log(1 + number of colonies grown on plates under the conditions used for panel A), as a function of the amount of silver nanoparticles in agar plates.

polyhedral plates) were more easily identified in other samples (Fig. 2B and C).

The presence of nanorods with an average edge length above 100 nm was confirmed by EFTEM. Figure 2B shows rod-shaped nanoparticles with mean edge lengths of 133 nm and mean diameters of 16 nm. In Fig. 2C, rod-shaped nanoparticles with larger aspect ratios, with a mean edge length of 192 nm and a mean diameter remaining at ~16 nm, can be seen.

Structural information on the truncated triangular nanoplates was obtained by oriented particulate monolayer X-ray diffraction (OPML-XRD). Figure 3 shows the XRD patterns of the nanoplates lying flat with their basal planes parallel to the substrate. The remarkably intensive diffraction peak at a 2θ value of 38.04 from the {111} lattice plane of face-centered cubic silver unequivocally indicates that the particles are made of pure silver and that their basal plane, i.e., the top crystal plane, should be the {111} plane (8). It has been suggested (8)

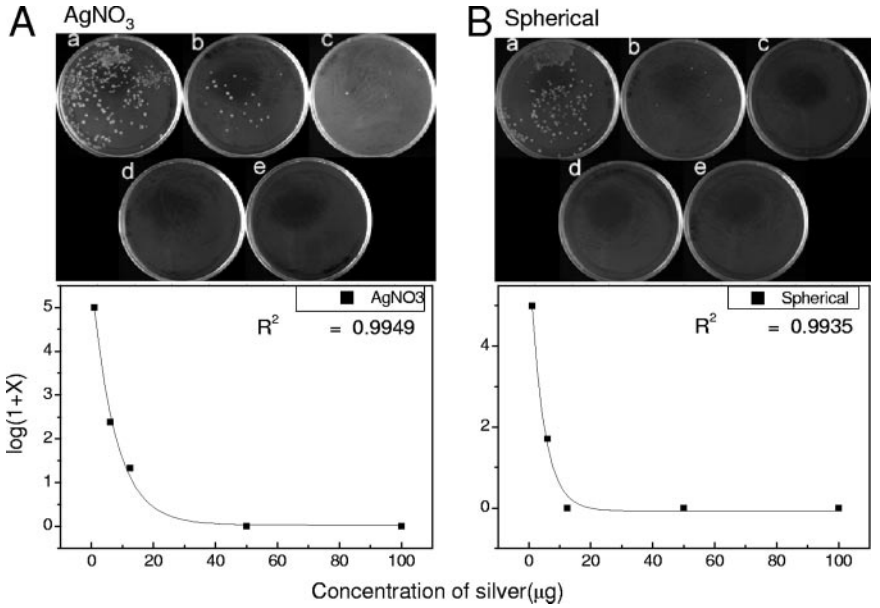

FIG. 5. Petri dishes initially supplemented with 10^5 CFU/ml of *E. coli* and incubated with silver at (a) 1, (b) 6, (c) 12.5, (d) 50, and (e) 100 μg and corresponding graphs showing log(1 + number of colonies grown on plates) as a function of the concentration of silver in agar plates. (A) Ag^+ (in the form of $AgNO_3$); (B) spherical silver nanoparticles.

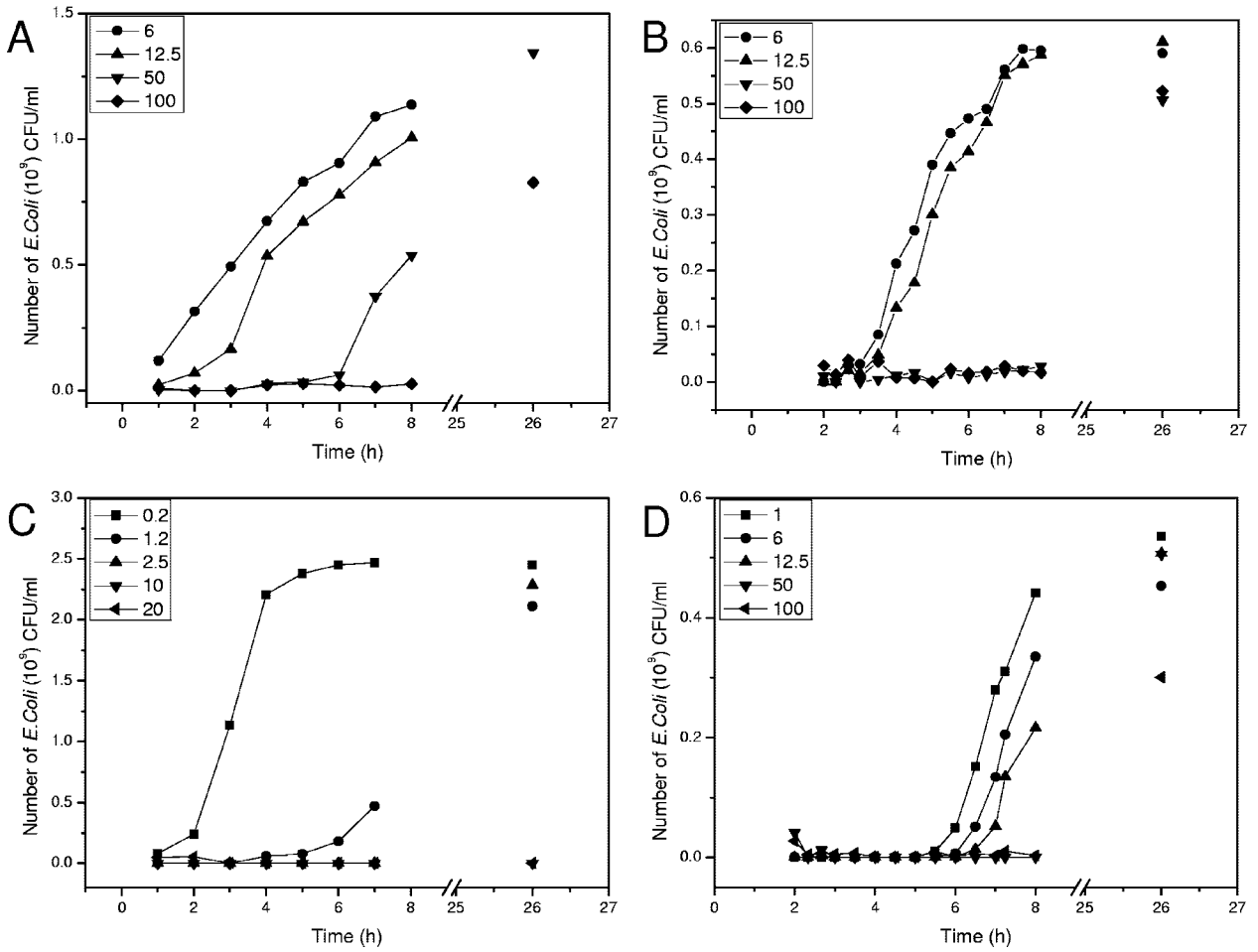

FIG. 6. Growth curve of *E. coli* in 100 ml NB with 10^7 CFU/ml in the presence of different concentrations of different silver nanoparticles. (A) $AgNO_3$; (B) spherical nanoparticles; (C) truncated triangular nanoparticles; (D) spherical nanoparticles with an initial bacterial concentration of 10^5 CFU/ml. Amounts (in micrograms) of silver nanoparticles are given in each panel.

that this plane may possess the lowest surface tension. Figure 3 (inset) shows the TEM image of purified truncated triangular particles with an average edge length of 40 nm.

Figure 4A shows plates to which a 100-μl bacterial suspension (approximately 10^7 CFU/ml) was applied. The presence of nanoparticles at a certain level inhibited bacterial growth by more than 90%. Interestingly, however, this level is significantly different for different nanoparticle shapes. For truncated triangular particles, almost complete inhibition of bacterial growth was observed even at a total silver content of 1 μg. In the case of spherical nanoparticles, a total silver content above 12.5 μg reduced the number of colonies significantly, while a total of 50 to 100 μg of silver caused 100% inhibition of bacterial growth. Rod-shaped nanoparticles and $AgNO_3$ showed inferior performance. Even in the presence of 100 μg of rod-shaped particles, some colonies grew on the plate, though fewer than with an identical $AgNO_3$ dose.

Figure 4B shows the corresponding results, expressed as $\log(1 + x) = f(c)$, i.e., $\log(1 + x)$ as a function of the total amount of silver nanoparticles (c), where x was the number of CFU grown on agar plates. The decrease in number of viable cells with increasing amounts of silver can be fitted with a first-order exponential decay curve with a nonlinear regression coefficient (R^2) ranging from 0.96 to 1.

Figure 5 displays the number of bacterial colonies grown in the presence of different amount of $AgNO_3$ and spherical nanoparticles when 100 μl (approximately 10^5 CFU/ml) of sample was applied to each plate. The results clearly indicate that at a given concentration of silver, inhibition of bacterial growth depends on the initial number of cells. An amount of 6 μg of spherical nanoparticles almost completely prevented bacterial growth (Fig. 5B). At silver (in the form of $AgNO_3$) amounts of 12.5 μg and above, 100% inhibition of bacterial growth was also observed (Fig. 5A). This is markedly different from the results obtained when the initial number of bacterial cells was 10^7 CFU. In this case also, the results, expressed as $\log (1 + x) = f(c)$, follow the first-order exponential decay curve with a nonlinear regression coefficient (R^2) of ~0.99 (Fig. 5).

The bacterial growth kinetics was monitored in 100 ml NB medium (initial bacterial concentration, 10^7 CFU/ml) supplemented with different amounts of different silver nanoparticles. Figure 6 clearly shows that at all amounts, the nanoparticles caused a growth delay of *E. coli*; increasing the concentration

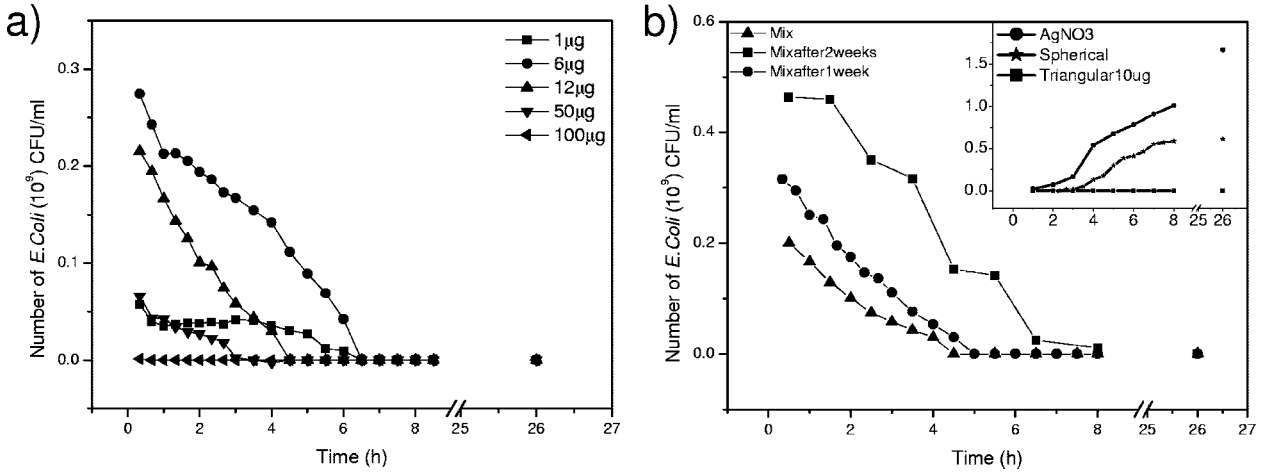

FIG. 7. (a) Killing activity for *E. coli* (in 100 ml NB supplemented with 10^7 CFU/ml) in the presence of a mixture of triangular, rod-shaped, and polyhedral silver nanoparticles (before purification), containing different amounts of total silver (Ag^+ and Ag nanoparticles) and CTAB. Total silver amounts are shown in each panel. (b) Decay curve of *E. coli* growth in 100 ml NB with 10^7 CFU/ml treated with the mother solution of truncated triangular and rod-shaped nanoparticles (total amount of silver, 12 μg). (Inset) Comparative graph of the dynamics of *E. coli* growth in the presence of 12 μg of spherical silver nanoparticles, 10 μg of triangular nanoparticles, and 12 μg of ionic silver ($AgNO_3$) in 100 ml NB supplemented with 10^7 CFU/ml. Axes and units for the inset are same as those for the main graph and have been omitted for simplicity.

of nanoparticles increased this growth delay. This is in line with findings reported previously (31). A trend similar to that seen in the plate study can be noticed in the broth study. At a given concentration, truncated triangular nanoparticles are found to be more effective in delaying the growth of *E. coli* than spherical particles, which again demonstrated better antibacterial activity than $AgNO_3$. A dose of 10 μg of truncated triangular particles completely inhibited growth even after 24 h (Fig. 6C), whereas 100 μg of silver (in the form of $AgNO_3$) and spherical nanoparticles caused only a prolonged growth delay, ~8 to 10 h (Fig. 6A and B).

As expected, bacterial growth was found to be dependent on the initial number of cells present in the broth. Figure 6D depicts the result of bacterial growth monitored in 100 ml of NB (initial cell numbers, 10^5 CFU/ml) supplemented with different doses of spherical silver nanoparticles. A comparison with Fig. 6B shows that spherical nanoparticles exhibited significantly superior antibacterial property at a given nanoparticle dose when the initial *E. coli* concentration was reduced. A similar trend was observed for other nanoparticles as well (data not shown).

Figure 7a depicts the killing activity for *E. coli* (in 100 ml of NB supplemented with 10^7 CFU/ml of cells) in the presence of the mother liquor (the reaction mixture of triangular, rod-shaped, and polyhedral silver nanoparticles, before centrifugation), containing different amounts of total silver (Ag^+ and Ag nanoparticles) as well as a substantial amount of CTAB. The killing activity was found to be sustained, as no cell growth was seen even after 26 h of incubation. Figure 7b shows the comparative killing activities for *E. coli* when the bacterial suspension was treated with the same mother liquor containing 12 μg of total silver immediately after preparation (see experimental section) and after 1 and 2 weeks of aging at room temperature. The killing activity of the silver hydrosol was found to diminish with increased aging time. The Fig. 7b inset shows the dynamics of *E. coli* growth as observed in the presence of 12 μg of different silver nanoparticles (10 μg of truncated triangular nanoparticles) and ionic silver ($AgNO_3$) in 100 ml of NB supplemented with 10^7 CFU/ml. Interestingly, instead of a growth curve (Fig. 7b, inset), as seen in the presence of purified silver nanoparticles, a decay curve was obtained when the *E. coli* suspension was treated with the unpurified mother solution of truncated triangular and rod-shaped nanoparticles, finally leading to complete killing of the bacterial cells.

The surface structures of both the untreated (Fig. 8A) and the treated bacterial cells (Fig. 8B) were examined using EFTEM. The treated bacterial cells were significantly changed, and major damage was observed in the outer membrane (Fig. 8C). Nanoparticles that accumulated in the membrane as well as some penetrating the cells can also be discerned in the EFTEM micrograph.

DISCUSSION

The size of metallic nanoparticles ensures that a significantly large surface area of the particles is in contact with the bacterial effluent. Considering a hypothetical case with spherical particles of uniform size, a reduction in the particle size from ~10 μm to 10 nm will increase the contact surface area by 10^9. Such a large contact surface is expected to enhance the extent of bacterial elimination. However, smallness in itself is not the goal. Synthesis and characterization of nanoscaled materials in terms of novel physicochemical properties is of great interest in the formulation of bactericidal materials.

Although growth on agar plates is a more ready means of distinguishing antimicrobial properties of silver nanoparticles of different shapes, in this study liquid-growth experiments showed basically similar results. But a previous study (31) pointed out a distinct difference between these two methods. In our study, complete inhibition of bacterial growth was observed on agar plates supplemented with nanoparticles (Fig. 4 and 5). It is noteworthy that inhibition depends on the con-

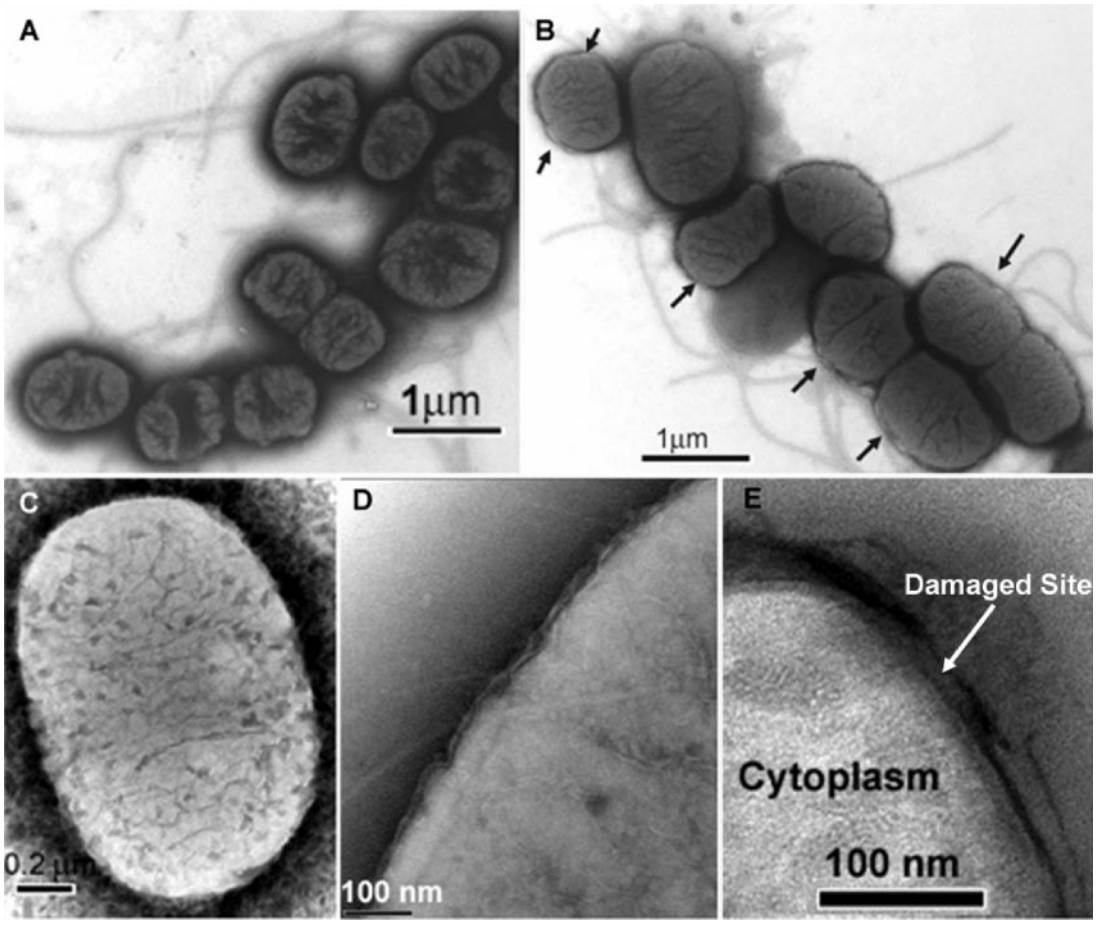

FIG. 8. EFTEM images of *E. coli* cells. (A) Untreated *E. coli*. Flagella can be seen. (B) *E. coli* grown on agar plates supplemented with Ag^+ ($AgNO_3$). Arrows indicate partially damaged membranes. These cells are viable. (C) *E. coli* treated with triangular silver nanoplates. Silver nanoparticles appear as dark irregular pits on the cell surface. (D) *E. coli* treated with spherical silver nanoparticles. (E) Enlarged image of part of the bacterial cell membrane treated with triangular silver nanoparticles. The cell membrane is damaged in multiple locations.

centration of the silver nanoparticles as well as on the initial bacterial number. On the other hand, silver nanoparticles in liquid medium, even at high concentrations, caused mainly a growth delay of *E. coli* (Fig. 6). Growth of bacterial cells resumed rapidly with a decrease in the concentration of nanoparticles. Sondi and Salopek-Sondi (31) showed that interaction of these particles with intracellular substances from the lysed cells caused their coagulation and the particles were thrown out of the liquid system.

The decay curves shown in Fig. 7a can be explained similarly. In the mother liquor of truncated triangular and rod-shaped nanoparticles, silver particles with different shapes were present in the micelles of the cationic quaternary ammonium surfactant CTAB. The surfaces of *E. coli* ATCC 10536 cells have a negative charge. Thus, the addition of a nanoparticle solution with a certain amount of cationic surfactant to the bacterial suspension probably led to coagulation of the nanoparticles via a charge neutralization mechanism. The low colloidal stability of the nanoparticles resulted in a decrease of effective silver concentration in the broth medium. However, most likely due to a synergistic effect of the cationic surfactant and silver nanoparticles, a decay curve was obtained, finally leading to complete cell death. Coagulation via a charge neutralization mechanism is most effective at an optimum coagulant dose under a particular set of experimental conditions (temperature, pH, and mixing speed). Most probably in our study, under the given experimental conditions, the nanoparticle levels of 6 to 12 μg correspond to the optimum surfactant concentration for effective coagulation, and a slower killing curve was obtained. At a level lower than the optimum nanoparticle level (and hence the optimum surfactant level) (e.g., 1 μg of silver), complete charge neutralization does not happen, whereas at a higher level (e.g., 50 or 100 μg), due to charge reversal the nanoparticles regain their colloidal stability, leading to poor or ineffective coagulation. Consequently, in those cases the killing is either much faster or immediate. A control experiment with the same amount of surfactant dose (but without silver nanoparticles) produced similar types of graphs (data not shown), though with a much lower killing rate, and confirmed the previous observations.

Reports on the mechanism of inhibitory action of silver ions on microorganisms show that upon Ag^+ treatment, DNA loses its replication ability (10) and expression of ribosomal subunit proteins as well as some other cellular proteins and enzymes

essential to ATP production becomes inactivated (40). It has also been hypothesized that Ag^+ primarily affects the function of membrane-bound enzymes, such as those in the respiratory chain (3, 23).

However, the mechanism of bactericidal actions of silver nanoparticles is still not well understood. In a previous report (31) on the bactericidal activity of silver nanoparticles, it was shown that the interaction between silver nanoparticles and constituents of the bacterial membrane caused structural changes in and damage to membranes, finally leading to cell death.

We speculate that the action of silver nanoparticles is broadly similar to that of silver ion. It may be anticipated that a bacterial cell in contact with silver nanoparticles takes in silver ions, which inhibit a respiratory enzyme(s), facilitating the generation of reactive oxygen species and consequently damaging the cell. The uptake of silver can be recognized by irregular pits (Fig. 8C). Silver (soft acid) has a greater tendency to react with sulfur- or phosphorus-containing soft bases, such as R-S-R, R-SH, RS^-, or PR_3. Thus, sulfur-containing proteins in the membrane or inside the cells and phosphorus-containing elements like DNA are likely to be the preferential sites for silver nanoparticle binding (3, 23). Figure 8C is an enlarged image of a part of a severely damaged cell membrane treated with truncated triangular silver nanoplates. It has been suggested (31) that disruption of membrane morphology may cause a significant increase in permeability, leading to uncontrolled transport through the plasma membrane and, finally, cell death.

Although the findings regarding interaction with *E. coli* were similar among nanoparticles with markedly different shapes, the inhibition results were not the same. The differences in the observed trends in *E. coli* inhibition can be explained in terms of the percent active facets present in nanoparticles of different shapes. The OPML-XRD pattern (Fig. 3) shows that the top basal plane of a truncated triangular nanoplate is a {111} surface. Spherical silver nanoparticles (generally with a cubooctahedral or multiple-twinned decahedral or quasi-spherical morphology) predominantly have {100} facets along with small percentage of {111} facets, while in case of the rod-like silver nanoparticles (e.g., pentagonal rods), side surfaces are bound by {100} and the ends by {111} facets (38). It has been demonstrated that the reactivity of silver is favored by high-atom-density facets such as {111} (1, 13). Morones et al. (25) proved the faceting of the particles as well as the direct interaction of the {111} facets with the bacterial surface. Thus, a high reactivity of the truncated triangular nanoplates, as found in this study, in comparison to other particles that contain fewer than {111} facets, like spherical or rod-shaped particles, is expected.

In conclusion, we have found that silver nanoparticles undergo shape-dependent interaction with the gram-negative bacterium *E. coli*. The interactions of silver nanoparticles with biosystems are just beginning to be understood, and these particles are increasingly being used as microbicidal agents. It may be speculated that silver nanoparticles with the same surface areas but with different shapes may also have different effective surface areas in terms of active facets. Though at present we are unable to give an estimation of how the surface areas of different nanoparticles influence their killing activity or to relate the bacterial killing capacity of silver nanoparticles with their effective surface areas, our results provide a basis for the measurement of shape-dependent bacterial activity of silver nanoparticles. However, it is imperative that the flexibility of nanoparticle preparation methods and their influence on other bacterial strains be explored.

ACKNOWLEDGMENT

This research was sponsored by the Korean Ministry of Science and Technology under contract M10640020002-06N4002-00211 ("A Study on Advanced Molecular Recognition Technology" program) with Seoul National University.

REFERENCES

1. **Ajayan, P. M., and L. D. Marks.** 1988. Quasimelting and phases of small particles. Phys. Rev. Lett. **60:**585–587.
2. **Bosetti, M., A. Masse, E. Tobin, and M. Cannas.** 2002. Silver coated materials for external fixation devices: in vitro biocompatibility and genotoxicity. Biomaterials **23:**887–892.
3. **Bragg, P. D., and D. J. Rainnie.** 1974. The effect of silver ions on the respiratory chains of *Escherichia coli*. Can. J. Microbiol. **20:**883–889.
4. **Brause, R., H. Moeltgen, and K. Kleinermanns.** 2002. Characterization of laser-ablated and chemically reduced silver colloids in aqueous solution by UV/VIS spectroscopy and STM/SEM microscopy. Appl. Phys. B **75:**711–716.
5. **Brigger, I., C. Dubernet, and P. Couvreur.** 2002. Nanoparticles in cancer therapy and diagnosis. Adv. Drug Delivery Rev. **54:**631–651.
6. **Burda, C., X. Chen, R. Narayanan, and M. A. El-Sayed.** 2005. Chemistry and properties of nanocrystals of different shapes. Chem. Rev. **105:**1025–1102.
7. **Callegari, A., D. Tonti, and M. Chergui.** 2003. Photochemically grown silver nanoparticles with wavelength-controlled size and shape. Nano Lett. **3:**1565–1568.
8. **Chen, S., and D. L. Carroll.** 2002. Synthesis and characterization of truncated triangular silver nanoplates. Nano Lett. **2:**1003–1007.
9. **Elechiguerra, J. L., J. L. Burt, J. R. Morones, A. Camacho-Bragado, X. Gao, H. H. Lara, and M. J. Yacaman.** 29 June 2005. Interaction of silver nanoparticles with HIV-1. J. Nanobiotechnol. **3:**6. http://www.jnanobiotechnology.com/content/3/1/6.
10. **Feng, Q. L., J. Wu, G. Q. Chen, F. Z. Cui, T. M. Kim, and J. O. Kim.** 2000. A mechanistic study of the antibacterial effect of silver ions on *Escherichia coli* and *Staphylococcus aureus*. J. Biomed. Mater. Res. **52:**662–668.
11. **Fresta, M., G. Puglisi, G. Giammona, G. Cavallaro, N. Micali, and P. M. Furneri.** 1995. Pefloxacine mesilate-loaded and ofloxacin-loaded polyethylcyanoacrylate nanoparticles—characterization of the colloidal drug carrier formulation. J. Pharm. Sci. **84:**895–902.
12. **Hamouda, T., M. Hayes, Z. Cao, R. Tonda, K. Johnson, W. Craig, J. Brisker, and J. Baker.** 1999. A novel surfactant nanoemulsion with broad-spectrum sporicidal activity against Bacillus species. J. Infect. Dis. **180:**1939–1949.
13. **Hatchett, D. W., and S. Henry.** 1996. Electrochemistry of sulfur adlayers on the low-index faces of silver. J. Phys. Chem. **100:**9854–9859.
14. **Hermanson, K. D., S. O. Lumsdon, J. P. Williams, E. W. Kaler, and O. D. Velev.** 2001. Dielectrophoretic assembly of electrically functional microwires from nanoparticle suspensions. Science **294:**1082–1086.
15. **Herrera, M., P. Carrion, P. Baca, J. Liebana, and A. Castillo.** 2001. In vitro antibacterial activity of glass-ionomer cements. Microbios **104:**141–148.
16. **Hranisavljevic, J., N. M. Dimitrijevic, G. A. Wurtz, and G. P. Wiederrecht.** 2002. Photoinduced charge separation reactions of J-aggregates coated on silver nanoparticles. J. Am. Chem. Soc. **124:**4536–4537.
17. **James, G. V.** 1971. Water treatment, 4th ed., p. 38. CRC Press, Cleveland, OH.
18. **Jana, N. R., L. Gearheart, and C. J. Murphy.** 2001. Wet chemical synthesis of high aspect ratio cylindrical gold nanorods. J. Phys. Chem. B **105:**4065–4067.
19. **Knoll, B., and F. Keilmann.** 1999. Near-field probing of vibrational absorption for chemical microscopy. Nature **399:**134–137.
20. **Kreibig, U., and M. Vollmer.** 1995. Optical properties of metal clusters. Springer, Berlin, Germany.
21. **Li, P., J. Li, C. Wu, Q. Wu, and J. Li.** 2005. Synergistic antibacterial effects of β-lactam antibiotic combined with silver nanoparticles. Nanotechnology **16:**1912–1917.
22. **Matsumura, Y., K. Yoshikata, S. Kunisaki, and T. Tsuchido.** 2003. Mode of bactericidal action of silver zeolite and its comparison with that of silver nitrate. Appl. Environ. Microbiol. **69:**4278–4281.
23. **McDonnell, G., and A. D. Russell.** 1999. Antiseptics and disinfectants: activity, action, and resistance. Clin. Microbiol. Rev. **12:**147–179.
24. **Mie, G.** 1908. Contributions to the optics of turbid media, especially colloidal metal solutions. Ann. Phys. **25:**377–445.
25. **Morones, J. R., J. L. Elechiguerra, A. Camacho, K. Holt, J. B. Kouri, J. T. Ramirez, and M. J. Yacaman.** 2005. The bactericidal effect of silver nanoparticles. Nanotechnology **16:**2346–2353.
26. **Mulvaney, P.** 1996. Surface plasmon spectroscopy of nanosized metal particles. Langmuir **12:**788–800.

27. **Novak, J. P., and D. L. Feldheim.** 2000. Assembly of phenylacetylene-bridged silver and gold nanoparticle arrays. J. Am. Chem. Soc. **122:**3979–3980.
28. **Oka, M., T. Tomioka, K. Tomita, A. Nishino, and S. Ueda.** 1994. Inactivation of enveloped viruses by a silver-thiosulfate complex. Metal-Based Drugs **1:**511.
29. **Oloffs, A., C. Crosse-Siestrup, S. Bisson, M. Rinck, R. Rudolvh, and U. Gross.** 1994. Biocompatibility of silver-coated polyurethane catheters and silver-coated Dacron® material Biomaterials **15:**753–758.
30. **Schatz, G. C., and R. P. Van Duyne.** 2002. Electromagnetic mechanism of surface-enhanced spectroscopy, p. 759–774. *In* J. M. Chalmers and P. R. Griffiths (ed.), Handbook of vibrational spectroscopy. Wiley, New York, NY.
31. **Sondi, I., and B. Salopek-Sondi.** 2004. Silver nanoparticles as antimicrobial agent: a case study on *E. coli* as a model for Gram-negative bacteria. J. Colloid Interface Sci. **275:**177–182.
32. **Sosa, I. O., C. Noguez, and R. G. Barrera.** 2003. Optical properties of metal nanoparticles with arbitrary shapes. J. Phys. Chem. B **107:**6269–6275.
33. **Stoimenov, P. K., R. L. Klinger, G. L. Marchin, and K. J. Klabunde.** 2002. Metal oxide nanoparticles as bactericidal agents. Langmuir **18:**6679–6686.
34. **Sun, Y. G., B. Mayers, T. Herricks, and Y. N. Xia.** 2003. Polyol synthesis of uniform silver nanowires: a plausible growth mechanism and the supporting evidence. Nano Lett. **3:**955–960.
35. **Sun, Y. G., B. Mayers, and Y. N. Xia.** 2003. Transformation of silver nanospheres into nanobelts and triangular nanoplates through a thermal process. Nano Lett. **3:**675–679.
36. **Tessier, P. M., O. D. Velev, A. T. Kalambur, J. F. Rabolt, A. M. Lenhoff, and E. W. Kaler.** 2000. Assembly of gold nanostructured films templated by colloidal crystals and use in surface-enhanced Raman spectroscopy. J. Am. Chem. Soc. **122:**9554–9555.
37. **Tokumaru, T., Y. Shimizu, and C. L. Fox.** 1984. Antiviral activities of silver sulfadiazine and ocular infection. Res. Commun. Chem. Pathol. Pharmacol. **8:**151–158.
38. **Wiley, B., Y. Sun, B. Mayers, and Y. Xia.** 2005. Shape-controlled synthesis of metal nanostructures: the case of silver. Chem. Eur. J. **11:**454–463.
39. **Wu, X., H. Liu, J. Liu, K. N. Haley, J. A. Treadway, J. P. Larson, E. Ge, F. Peale, and M. P. Bruchez.** 2003. Immunofluorescent labeling of cancer marker Her2 and other cellular targets with semiconductor quantum dots. Nat. Biotechnol. **21:**41–46.
40. **Yamanaka, M., K. Hara, and J. Kudo.** 2005. Bactericidal actions of a silver ion solution on *Escherichia coli*, studied by energy-filtering transmission electron microscopy and proteomic analysis. Appl. Environ. Microbiol. **71:**7589–7593.
41. **Zhou, Y., S. H. Yu, X. P. Cui, C. Y. Wang, and Z. Y. Chen.** 1999. Formation of silver nanowires by a novel solid-liquid phase arc discharge method. Chem. Mat. **11:**545–546.